



# Buckling Resistance of Axially Loaded Cold-Formed Steel Compound Sections: Numerical Simulation and Assessment of Codified Design Approach

Jing-Ren Wu<sup>1</sup> · Luigi Di Sarno<sup>1</sup> · Steve Hesketh<sup>2</sup> · Nigel Phan<sup>2</sup>

Received: 15 December 2021 / Accepted: 12 July 2022  
© The Author(s) 2022

## Abstract

The practical application of cold-formed high strength steel is becoming increasingly popular in structural engineering due to its great efficiency and cost effectiveness. However, cold-formed steel sections are usually associated with high slenderness, hence are susceptible to buckling failure. Consequently, the buckling resistance of steel struts made of cold-formed high strength steel must be determined with carefulness, particularly for complex compound sections. To this end, the present paper aims at investigating the behaviour of back-to-back channel sections made of S700 steel with a characteristic yield strength of 700 MPa. Compressive tests on such members are conducted for the purpose of validating the finite element models. Subsequently, a numerical parametric analysis is carried out on the buckling resistance of axially loaded cold-formed steel back-to-back channel sections, using the previously validated numerical modelling approach. In particular, the effects of stiffeners and number of bolts on the buckling resistance are investigated. Furthermore, the results of the parametric analysis are also compared with the codified buckling resistance determined based on the effective width method adopted in Eurocode 3 Part 1–3, in order to evaluate the reliability of the standardised design method for buckling resistance.

**Keywords** Finite element modelling · Cold-formed steel · Compound section · Number of bolts · Standardised design method · Temporary works

## Abbreviations

$A_{eff}$	Effective area of the cross-section
$A_g$	Area of the gross cross-section
$F_{cr}$	Critical buckling load
$f_y$	Yield strength of steel
$I$	Second moment of area of the gross cross-section
$I_t$	Torsion constant of the gross cross-section

$I_w$	Warping constant of the gross cross-section
$i_y$	Radius of gyration in the y-y direction of the gross cross-section
$i_z$	Radius of gyration in the z-z direction of the gross cross-section
$L$	Length of member
$l_T$	Effective length for torsional buckling
$P_{ne}$	Buckling resistance for yielding or global buckling
$P_{nl}$	Buckling resistance for local buckling
$P_{nd}$	Buckling resistance for distortional buckling
$P_{num}$	Buckling load estimated by numerical models
$S$	Spacing of bolts
$t$	Thickness of CFS section
$y_0$	Y-coordinate of the shear centre of the gross cross-section
$z_0$	Z-coordinate of the shear centre of the gross cross-section
$\bar{\lambda}$	Non-dimensional slenderness defined in EC3
$\lambda_c$	Slenderness as defined in AISI
$\chi$	Reduction factor as in EC3 to determine the buckling resistance

---

✉ Jing-Ren Wu  
jingren.wu@liverpool.ac.uk

Luigi Di Sarno  
luigi.di-sarno@liverpool.ac.uk

Steve Hesketh  
steve.hesketh@mgf.co.uk

Nigel Phan  
nigel.phan@mgf.co.uk

<sup>1</sup> Department of Civil Engineering and Industrial Design, School of Engineering, University of Liverpool, Liverpool, UK

<sup>2</sup> Engineering Centre, Foundation House, Wallwork Road, Astley, Manchester M29 7JT, UK

## 1 Introduction

The application of cold-formed steel (CFS) is attracting increasing attention in the field of structural engineering, such as temporary works, steel decks, etc. The major advantages of CFS sections are that they are lightweight, hence are easy to handle on site, and that they have high strength-to-weight ratio, in particular when high strength steel is utilised, hence can lead to great structural efficiency and material optimization, which in turns, is in line with sustainable material utilization and green economy. However, the light weight of CFS sections also means that they tend to be thin-walled structures, which brings about the major challenge of designing CFS sections, as they are very susceptible to various types of buckling failure. Potential buckling modes of CFS sections include local buckling, distortional buckling, flexural buckling, torsional buckling and torsional-flexural buckling. The last three modes are also referred to as the global buckling modes. Different buckling modes can occur simultaneously and interact between each other. Thus, it is essential to properly account for the complicated response of CFS sections in order to obtain a safe design of their buckling resistance.

Among the typical profiles used for CFS sections, channel sections are one of the most widely used profiles in the steel manufacturing industry. In the past few decades, numerous previous work has been conducted investigating the behaviour of single channel sections subjected to buckling failure. Some representative studies include Rasmussen and Hancock (1994) and Young and Rasmussen (1998a) on the behaviour of plain channel sections, as well as Young and Rasmussen (1998b) and Becque and Rasmussen (2009) on lipped channel sections. Moreover, many other research has been performed on more complex channel sections, such as Kesti and Davies (1999), Yan and Young (2002), Yang and Hancock (2004), Kwon et al. (2009), etc.

More recently, however, the focus of research has switched from single channel sections to more complex compound sections. Compound sections can usually be more advantageous than single sections as they tend to have symmetric shapes, and consequently have no eccentricities between shear and gravity centres, hence exhibit higher member stability (Craveiro et al., 2016). The behaviour of compound channel sections have been investigated in many previous studies. Some of the studies, such as Zhang and Young (2012), Ghannam (2017), Roy et al. (2018a, b) and Ting et al. (2018) on the back-to-back compound channel sections, have focused on the open compound sections. On the other hand, there are also a few studies performed on the closed compound sections, including Shu et al. (2013), Roy et al., (2019a, b) and

Rahnavard et al. (2021). Moreover, some other studies have also been carried out concerning the influence of web openings, such as Lian et al., (2016a, 2016b) and Chen et al. (2019).

Along with the rapid development of CFS members, their associated standardised design procedures have also been provided, which can be categorised into two different methods, namely the *Effective Width Method* and the *Direct Strength Method*. The former method is adopted worldwide, including in the European Standard EN 1993-1-1 (CEN, 2005) and EN 1993-1-3 (CEN, 2006), whilst the latter is currently adopted in the American Standard AISI 100-16 (AISI, 2016) and the Australian/New Zealand code AS/NZS 4600 (SA, 2018). The Direct Strength Method, proposed by Schafer and Peköz (1998) and Hancock et al. (2001), is considered an advanced alternative to the conventional Effect Width Method, which is aimed at determining the resistance of CFS members with increasingly complex profiles.

Despite large amount of effort has been put into the research of CFS members, it is worth highlighting that the majority of previous research only involved CFS members made of steel with yielding strength up to 500 MPa. However, the number of studies concerning high-strength CFS members, which usually have yield strength over 700 MPa, are very limited. Since nowadays the manufacturing of high-strength steel is becoming more and more mature, the application of high-strength CFS members is attracting growing attention from the industry, and issues concerning the use of high-strength steel should be addressed. Firstly, there is inadequate experimental test performed to investigate the buckling resistance of high-strength CFS members with complex profiles. Besides, the accuracy of current standardised design procedures requires evaluation, as there is also a lack of studies assessing the capability of codified methods to estimate the resistance of high-strength CFS members in literature. Despite a few studies have conducted evaluations of the current European design approach, such as Haidarali and Nethercot (2012), Chan et al. (2015) and Ye et al. (2018), they were not dealing with the application of high-strength steel in compound sections. Therefore, it is of interest to fill the gap by conducting experimental and numerical investigation of the behaviour of high-strength CFS members, and evaluate the reliability of codified design methods in this regard.

The present paper is aimed at investigating the buckling resistance of back-to-back channel sections made of S700 steel (i.e. yield strength equal to 700 MPa) under compressive loading through numerical parametric analysis, and conducting preliminary evaluation of the reliability of the current European design method. Experimental tests were performed initially for the purpose of calibrating and validating the finite element (FE) models. Subsequently, the parametric analysis was carried out, which involved a wide

range of member slenderness. The objectives of the parametric analysis are firstly to investigate the effects of spacings between bolts and on the buckling resistance of the compound sections, and secondly to compare the numerical results with the design buckling resistance, thus the reliability of codified design methods can be evaluated.

## 2 Comparisons Between the European and American Standardised Design Methods

A brief comparison between the European and American Codified design methods is present herein. The European codified design method refers to the Effective Width Method summarised in EN 1993 (CEN, 2006) while the American design method refers to the Direct Strength Method provided in AISI 100–16 (AISI, 2016). The two methods are respectively referred to as the EC3 and AISI method in the rest part of this paper. It should be noted that for convenience, the notations used in the analytical formulae have been adapted to be consistent between the two design methods, hence are not necessarily the same as the notations used in each of the standards.

Both of the EC3 and AISI methods deal with the global buckling modes, *i.e.* flexural buckling, torsional buckling and torsional-flexural buckling, in a similar manner, as demonstrated by the formulae summarised in Table 1. As shown in Eq. (1), both methods adopt the concept of member slenderness and apply a reduction factor to the resistance of cross-section under compression (also referred to as the squash load  $P_y$  in the AISI method). One of the major differences between the two design methods is that in the EC3 method, the slenderness (denoted as  $\bar{\lambda}$ ) depends on the

effective area of cross-section, whilst in the AISI method the slenderness (denoted as  $\lambda_c$ ) depends on the gross cross-section, as illustrated by Eq. (2). Correspondingly, the two methods utilise different relations between the reduction factor and the slenderness of members. For example, EC3 describes the reduction factor  $\chi$  as a function of the slenderness  $\bar{\lambda}$  via five different buckling curves, as shown in Fig. 1, which are derived for different shapes of cross-sections. In particular, when  $\bar{\lambda}$  is smaller than 0.2, no reduction is adopted as global buckling is not considered likely to occur. On the other hand, the AISI method provides explicit formulae to describe the relation between the global buckling load ( $P_{ne}$ ) and the squash load ( $P_y$ ), as shown in Eq. (1). Nevertheless, it is worth mentioning that both methods adopt equivalent analytical formulae to determine the critical buckling load ( $F_{cr}$ ) associated with each global buckling mode, as summarised in Eqs. (3) to (5), which are essential in the calculation of the member slenderness.

Other major differences between the EC3 and the AISI methods are related to the ways of accounting for the effects of local and distortional buckling, as demonstrated in Table 2. In principle, the EC3 method utilises the effective

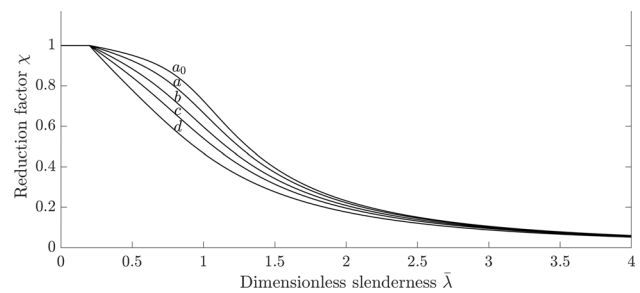


Fig. 1 Design buckling curves adopted in the EC3

Table 1 Comparisons between the EC3 and AISI method of designing for global buckling

	EC3	AISI
General formula	$P_{ne} = \frac{\chi A_{eff} f_y}{\gamma_{M1}}$ <p>See Fig. 1 for the relation between <math>\chi</math> and <math>\bar{\lambda}</math></p>	$P_{ne} = \begin{cases} (0.658\lambda_c^2) P_y, \lambda_c \leq 1.5 & (1) \\ (0.877/\lambda_c^2) P_y, \lambda_c > 1.5 \end{cases}$ <p>where <math>P_y = A_g f_y</math></p>
Slenderness	$\bar{\lambda} = \sqrt{\frac{A_{eff} f_y}{F_{cr}}}$	$\lambda_c = \sqrt{\frac{A_g f_y}{F_{cr}}} & (2)$
Flexural	$F_{cr,FL} = \frac{\pi^2 EI}{L_{cr}^2} & (3)$	
Torsional	$F_{cr,T} = \frac{1}{i_0^2} \left( GI_t + \frac{\pi^2 EI_w}{L_{cr}^2} \right)$ <p>where <math>i_0^2 = i_y^2 + i_z^2 + y_0^2 + z_0^2</math></p>	$& (4)$
Flexural–torsional	$F_{cr,TF} = \frac{F_{cr,FLy}}{2\beta} \left[ 1 + \frac{F_{cr,T}}{F_{cr,FLy}} - \sqrt{\left( 1 - \frac{F_{cr,T}}{F_{cr,FLy}} \right)^2 + 4 \left( \frac{y_0}{i_0} \right)^2 \frac{F_{cr,T}}{F_{cr,FLy}}} \right]$ <p>where <math>\beta = 1 - \left( \frac{y_0}{i_0} \right)^2</math></p>	$& (5)$

**Table 2** Comparisons between the EC3 and AISI method of designing for local and distortional buckling

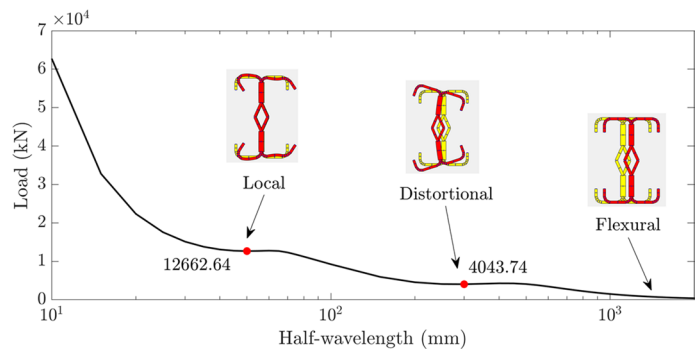
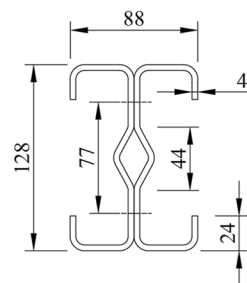
	EC3	AISI
Local buckling	Effective width of cross-sectional components	For $\lambda_l \leq 0.776$ : $P_{nl} = P_{ne}$ For $\lambda_l > 0.776$ : $P_{nl} = \left[ 1 - 0.15 \left( \frac{P_{cr,l}}{P_{ne}} \right)^{0.4} \right] \left( \frac{P_{cr,l}}{P_{ne}} \right)^{0.4} P_{ne}$ where $\lambda_l = \sqrt{P_{ne}/P_{cr,l}}$
Distortional buckling	For $\bar{\lambda}_d \leq 0.65$ : $\chi_d = 1.0$ For $0.65 < \bar{\lambda}_d < 1.38$ : $\chi_d = 1.47 - 0.723\bar{\lambda}_d$ For $\bar{\lambda}_d \geq 1.38$ : $\bar{\lambda}_d = \sqrt{f_{yb}/\sigma_{cr,s}}$	For $\lambda_d \leq 0.561$ : $P_{nd} = P_y$ For $\lambda_d > 0.561$ : $P_{nd} = \left[ 1 - 0.25 \left( \frac{P_{cr,d}}{P_y} \right)^{0.6} \right] \left( \frac{P_{cr,d}}{P_y} \right)^{0.6} P_y$ where $\lambda_d = \sqrt{P_y/P_{cr,d}}$

width method to reduce the width of cross-sectional components, as well as a distortional slenderness  $\bar{\lambda}_d$  to reduce the thickness of edge and intermediate stiffeners. Thus, an effective area of the gross cross-section can be obtained and used in the general formula in Table 1. On the other hand, the AISI method deals with the local and distortional buckling in a similar manner to the global buckling, where two additional slenderness  $\lambda_l$  and  $\lambda_d$  are utilised, leading to the local buckling load ( $P_{nl}$ ) and the distortional buckling load ( $P_{nd}$ ). The minimum of the buckling load associated with local, distortional and global buckling will then be adopted as the buckling load of the cross-section. It should be mentioned that in the present study, the critical local ( $P_{cr,l}$ ) and distortional ( $P_{cr,d}$ ) buckling loads defined in the AISI method are determined through elastic buckling analysis rather than the analytical approach provided in the AISI standard.

### 3 Description of the CFS Channel

The CFS channel section involved in the present study is a back-to-back compound channel section, whose buckling behaviour under axial compressive loading was investigated. The compound section is made of S700 steel with a characteristic yield stress of 700 MPa. Detailed dimensions of the open compound section are presented in Fig. 2, which consists of two channel sections with edge and intermediate stiffeners. The compound section has an overall dimension of  $88 \times 128$  mm, and has a uniform thickness of 4 mm. The channel sections are connected to each other via two rows of M6 bolts, as indicated by the dash lines across the section webs in Fig. 2. It should also be mentioned that the compound section was purposely designed to be not susceptible to local and distortional buckling according to the EC3 design approach, *i.e.* the effective area of such cross-section is approximately equal to  $1880 \text{ mm}^2$ , which is slightly less than the gross cross-sectional area of  $1907 \text{ mm}^2$ , mainly due

**Fig. 2** The back-to-back CFS channel section investigated in the present study (unit: mm) and its buckling load-half-wavelength curve obtained from CUFSM (Schafer, 2020)



to the reduction in the thickness of stiffeners to account for the limited effects of distortional buckling.

Figure 2 also shows the curve of buckling load against half-wavelength for the compound section obtained from CUFSM (Schafer, 2020). It is shown that the elastic critical local and distortional buckling loads of this compound section are determined to be around 12,662.64 and 4043.74 kN, corresponding to a critical half-wavelength of around 50 and 300 mm, respectively. The results shown in the curve will then be adopted in the implementation of the AISI design approach in the following part of this study. Notably, based on the critical buckling loads, the associated slenderness  $\lambda_l$  and  $\lambda_d$  were found to be respectively smaller than 0.776 and 0.561, hence no reduction was required to account for the effects of local and distortional buckling, which was consistent with the aforementioned design targets.

### 4 Experimental Tests and Validation of Numerical Models

#### 4.1 Test Specimens and Setup

Axial compressive tests were conducted on the 1:2 scaled specimens of the channel sections introduced in Sect. 3 for the purpose of model validation. Considering the capacity

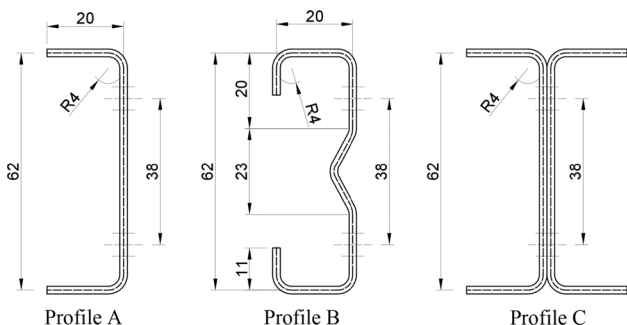


Fig. 3 Dimension of the 1:2 scaled channel sections tested in the laboratory

Table 3 List of test specimens and comparisons of their estimated and measured buckling load

Specimen Label	Profile	L (mm)	t (mm)	Buckling mode*		Buckling load		Error (%)
				Num	Exp	$P_{Num}(kN)$	$P_{Exp}(kN)$	
1	A	250	2	L	L	122.12	116.60	4.73
2	B	250	2	DT	DT	156.58	167.63	- 6.59
3	B	500	2	DT	DT	143.71	140.51	2.28
4	B	750	2	DT+FL	DT+FL	119.37	121.03	- 1.37
5	B	1000	2	FL	FL	88.33	95.08	- 7.05
6	C	1000	2		FL	188.84 (A)	197.10	- 4.18
					FL	186.96 (B)		- 5.14

\*L local buckling; DT distortional buckling; FL flexural buckling

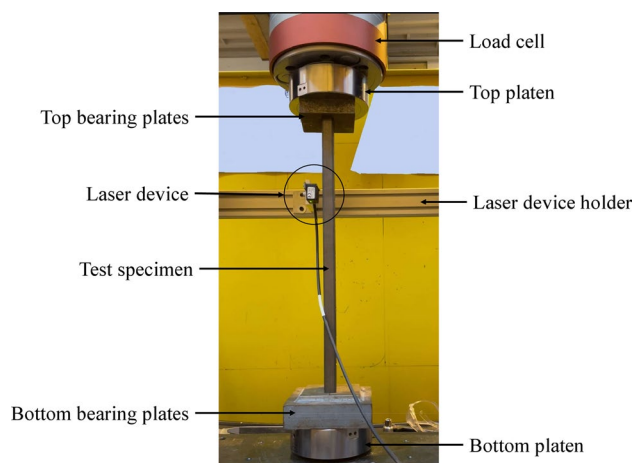


Fig. 4 Setup of the compressive test of the CFS channels

of the available test machine in the laboratory, the model validation had to be done implicitly, based on single channel channels with and without stiffeners, as well as an unstiffened compound section for the calibration of the effects of bolt connections. The profiles of the strut members tested in the lab are presented in Fig. 3, which are referred to as test profile “A”, “B” and “C”. As can be seen in Fig. 3, the single channel sections had a centreline dimension of 62 × 20 mm and the cross-sectional thickness was 2 mm, while the unstiffened compound section was the back-to-back built-up section of the single unstiffened channel section. Table 3 contains a list of the test specimens, where a total of six CFS channels were tested in the lab. It is worth mentioning that in the case of the scaled back-to-back unstiffened channel sections, two rows of M3 bolts were used to connect the two channels together at a spacing of 38 mm along the web and 50 mm along the member length. It is also worth noting that, the single channel specimens (Profile A and B) also had holes of 6 mm in diameter in their webs, which were cut in order to accommodate the bolts.

The specimens were loaded by an Universal Testing Machine system with a capacity of 250 kN, as shown in



Fig. 4, in accordance with the requirements in the international testing standard ASTM E9 (ASTM International, 2019). Each specimen was carefully placed on the flat platen at the bottom with its centroid in alignment with the centre of the loading cell. The transverse movement of the ends of the specimens were restrained by the high pressure, hence high frictional forces between the end cross-sections and platens, which, prior to the occurrence of buckling, is close to a fixed boundary condition. It is noteworthy that, as highlighted in Fig. 4, a laser device was also utilised during the test to measure the end shortening of the specimens, which was in reality equal to the sum of the axial deformation of the test specimens and the slight penetration of the test specimens into the bearing plates at the top and the bottom.

It should be noted that due to limitation of available test equipment, it was not feasible to measure the true profile of imperfection of the specimens prior to the compressive tests. In addition, as the main purpose of the experiments was for the calibration of numerical model, a simple testing scheme was adopted where each specimen was tested once subjected to monotonic loading until failure occurred. The monotonic compressive load was applied to the specimens through displacement control at a strain rate equal to 0.5% per minute, and loading was terminated when a significant drop in load was observed. At the end of tests, the axial load–displacement curve of each specimen was extracted from the test machine and the laser device.

## 4.2 Numerical Modelling of the CFS Channels

Nonlinear finite element (FE) models of the CFS channels were developed in the commercial software ABAQUS (Dassault Systemes, 2014). Centreline dimensions were adopted to build the models of the channel sections, while two methods were utilised to simulate the influence of bolts.

Fig. 5 Modelling of the channel sections in ABAQUS

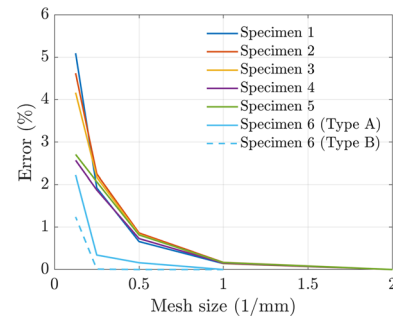
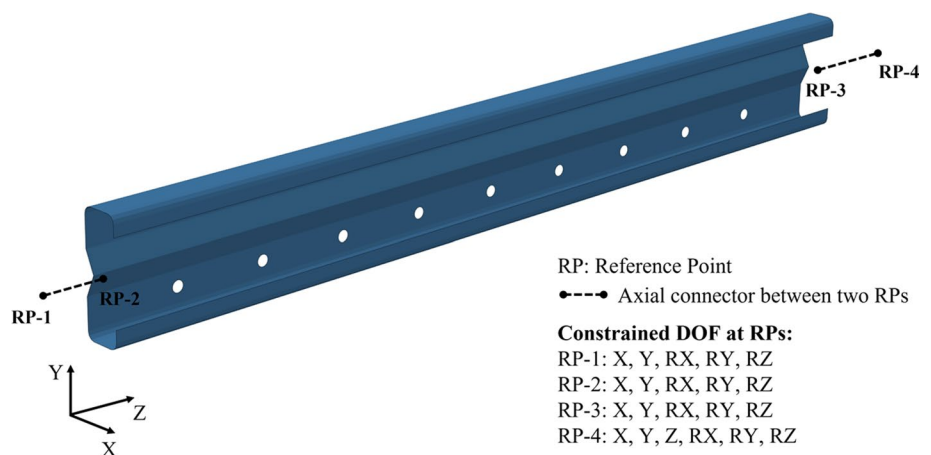


Fig. 6 Sensitivity analysis on the mesh size

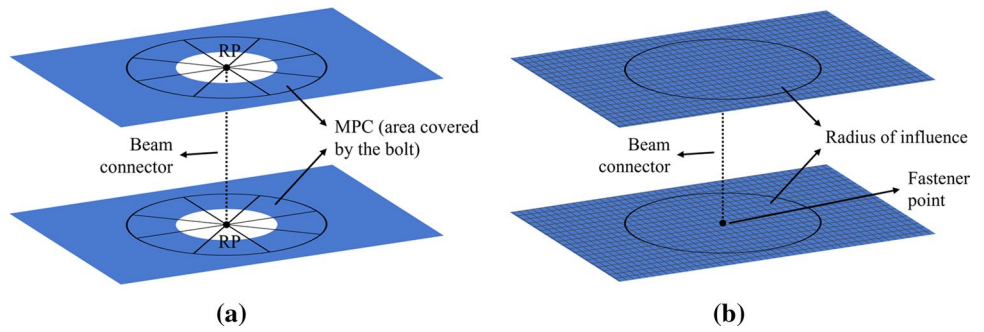
### 4.2.1 Material Properties

The specimens were manufactured using S700 high strength steel, which has a nominal yield stress of 700 MPa. However, due to lack of material tests, the properties of the S700 steel were defined based on the findings by Shakil et al. (2020). As a result, the Young's modulus of steel was assumed to be 216 GPa and the Poisson's ratio was 0.3. Besides, the yield and ultimate stress of the S700 steel was assumed to be 764 and 839 MPa, respectively, with a 11.2% elongation at the ultimate stress.

### 4.2.2 Elements and Mesh

The CFS channel members were modelled using the S4R shell element, which is a four-node general-purpose shell element with reduced integration point and is able to account for finite membrane strains and arbitrarily large rotation. Examples of the FE models are presented in Fig. 5. It is worth mentioning that axial connectors were added to the ends of each CFS members to account for the elastic deformation of the bearing plates used in the compressive test, as demonstrated in Fig. 5, where the two axial connectors were in series with the CFS member (Fig. 6). The stiffness of the

**Fig. 7** Illustration of the simplified modelling approach of bolts: **a** the MPC and beam connector approach (Type A); **b** the mesh-independent fastener approach (Type B)



axial connector was calibrated to be approximately  $EA/h_{bp}$ , where  $h_{bp}$  is the height of the bearing plate. However, it should also be noted that the axial connectors were only included in the FE models for validation purpose, and were not included in the successive numerical parametric analysis.

A preliminary sensitivity analysis on the mesh size was conducted on each channel members tested in this study, which investigated the impact of mesh size on the critical buckling load determined by elastic buckling analysis. The result of the sensitivity analysis was presented in Fig. 7, where the error was defined as the difference between the critical buckling estimated by each mesh size considered and that predicted with mesh size equal to 0.5 mm (1 mm in the case of specimen 6). As can be seen in Fig. 7, with a mesh size equal to 2 mm all FE models were able to reduce the error to be within 1%, therefore, a mesh size of 2 mm was adopted for all the analysis in this section.

### 4.2.3 Modelling of Bolts

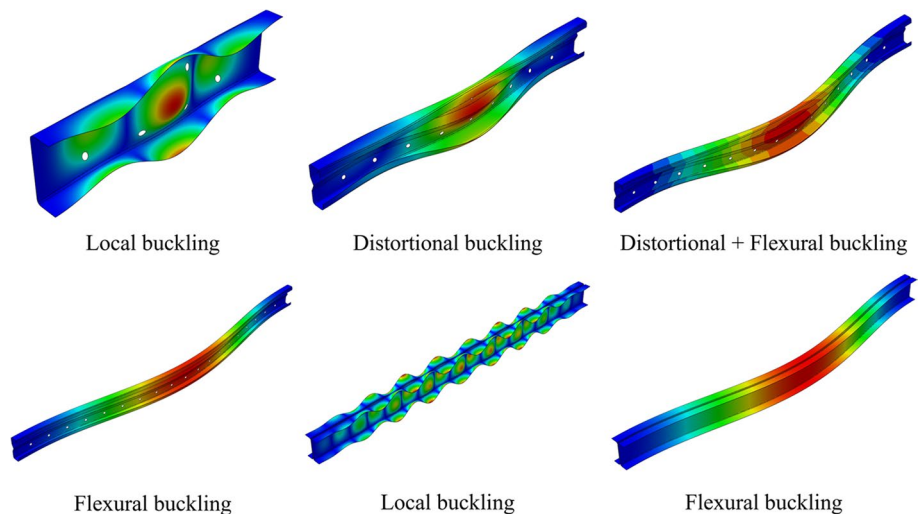
In the present study, two methods were adopted to simulate the effects of bolts, as shown in Fig. 7, which are referred to as Type A and Type B approach, respectively. Type A approach simulated the bolts through beam connectors and

Multi-point Constraints (MPCs), as illustrated in Fig. 7a, which included physically a hole in the model. Each MPC covered an area of 6 mm in radius, which was equal to the area covered by the bolt head and nut (approximately twice the size of the hole). On the other hand, Type B approach adopted the mesh-independent fastener generated by Abaqus with beam connectors, as shown in Fig. 7b, which was considered a simplified way of modelling bolts compared to the Type A approach. The holes were not necessary to be built in the Type B approach. It is noteworthy that bolts were not damaged or loosened during the test, hence rigid behaviour was assumed for the bolts in this study.

### 4.2.4 Boundary Conditions, Constraints and Contacts

Boundary conditions were applied to all the four reference points in each FE model. As indicated in Fig. 5, RP-1, RP-2 and RP-3 was only able to move in the axial direction of the member, while the fixed boundary condition was applied to RP-2. In the meantime, the end sections of each member was constrained by RP-2 and RP-3 through the ‘Beam’ MPCs. In addition, surface-to-surface contact with ‘Hard’ normal behaviour was also defined in the models of the compound

**Fig. 8** Representative buckling mode shapes of the test specimens



channel sections to model the interaction between the web of each channel.

#### 4.2.5 Geometric Imperfection

The amplitudes of geometric imperfection of the tested CFS members were not measured, consequently, the amplitudes recommended in literature was adopted. The shape of geometric imperfection were assumed to be based on the combination of global and local buckling modes. Some representative buckling modes of the tested CFS members were presented in Fig. 8, covering the local, distortional and flexural buckling modes of the test specimens. It is worth mentioning that the stiffened channel members involved in the test all had a combined distortional and flexural buckling mode as their first buckling mode, hence the distortional buckling mode was not explicitly included in the definition of geometric imperfection. The amplitude of global imperfection was assumed to be equal to  $L/1100$  according to Dabaon et al., (2015a, 2015b) while the amplitude of local imperfection was assumed to be equal to 0.5% of the

thickness of the cross-section, based on the study by Ellobody and Young (2005).

#### 4.2.6 Analysis Procedure

For each model, a linear buckling analysis was firstly performed to extract the buckling mode shapes, which was aimed at defining the initial geometric imperfection of the CFS members, using the aforementioned approach. Successively, the buckling behaviour of each test specimen was numerically simulated based on the *Riks* method, where the results were compared with the experimental measurements for the purpose of model validation.

#### 4.2.7 Analysis Procedure

For each model, a linear buckling analysis was firstly performed to extract the buckling mode shapes, which was aimed at defining the initial geometric imperfection of the CFS members, using the aforementioned approach. Successively, the buckling behaviour of each test specimen was numerically simulated based on the *Riks* method, where the results were compared with the experimental measurements for the purpose of model validation.

### 4.3 Comparison Between the Numerical Simulation and Test Results

The measured and estimated buckling load of each test specimen was summarised in Table 3. It can be seen that the estimation of buckling load is in good agreement with the measured values, with the differences being generally smaller than 10%. Besides, the estimated critical buckling modes based on elastic buckling analysis, which were adopted to define the imperfection of the FE models, were also summarised in Table 3, along with the observed buckling modes

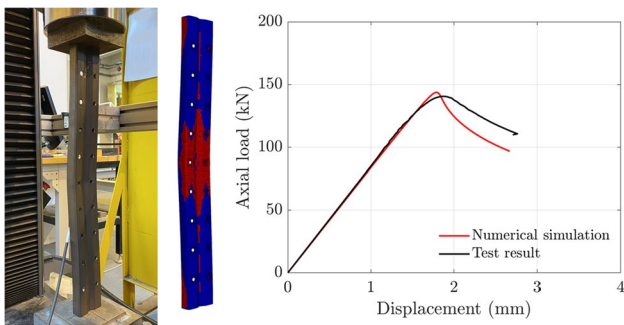
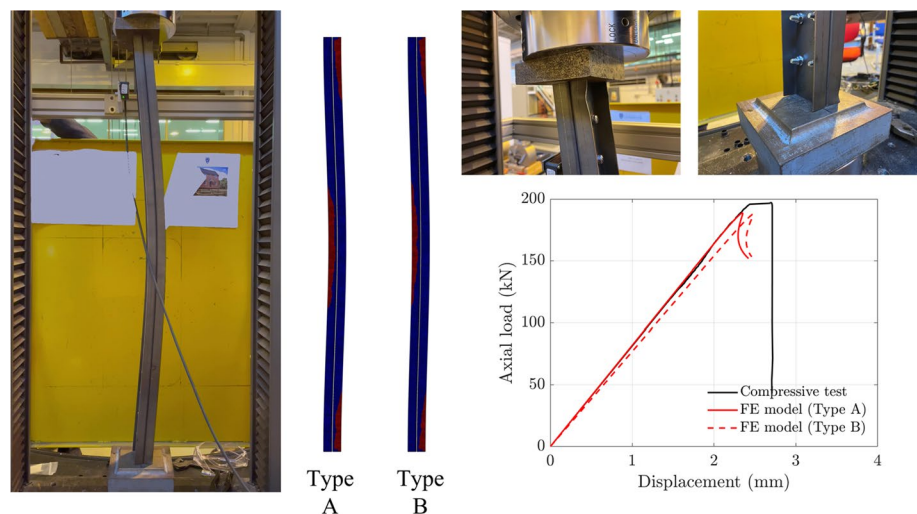


**Fig. 9** Failure mode and force–displacement curve of Specimen 3: comparison of the damage mode and the axial load–displacement curve

**Fig. 10** Failure mode and force–displacement curve of Specimen 6: comparison of the damage mode and the axial load–displacement curve





during the tests. It can be seen that good agreement was also achieved in terms of the buckling modes. Additionally, it is also indicated in Table 3 that the two approaches of modelling bolts yielded very similar estimates of the buckling load of Specimen 6.

Aside from the buckling load, comparisons were also made between the estimated and observed failure mode. Two examples of the FE model validation are presented herein to demonstrate the comparisons. Figure 9 shows the validation of the FE model of Specimen 3. It can be seen that the FE model obtained a similar failure mode to that observed during the test, where failure was primarily due to the combination of distortional buckling and flexural buckling, causing massive yielding in the middle of the specimen. Besides, the force–displacement curves also demonstrates that good agreement was achieved between the elastic axial stiffness of the strut.

Another example is provided in Fig. 10, which shows the behaviour of Specimen 6. It is shown that the FE model of the back-to-back channel section was able to capture correctly the response of the specimen. As can be seen in Fig. 10, flexural buckling and local buckling were noticed on the specimen, which was consistent with the damage predicted by the FE model, as yielding was mainly found at the middle of the specimen and at the compressive flanges near both ends. Moreover, as also shown in Fig. 10, the two modelling approaches of bolts yielded two similar response curves of the specimen, except that the stiffness estimated by Type B approach was slightly lower than that estimated by Type A approach. However, as previously mentioned, the two types of the modelling approaches provided close predictions of the buckling load, and since Type B approach is more simplified and easier to be implemented, it can be used in the following parametric analysis of the present study.

**Table 4** Buckling load of the back-to-back compound channel sections (fixed ends)

Label	EC3	AISI	$P_{design}(kN)$		$P_{num}(kN)$		
	$\bar{\lambda}$	$\lambda_c$	EC3	AISI	S=100 mm	S=200 mm	S=400 mm
F800	0.33	0.33	1281.69	1274.83	1366.14	1305.84	1298.75
F1200	0.49	0.50	1191.08	1203.77	1350.96	1319.67	1272.44
F1600	0.66	0.67	1081.12	1110.88	1265.35	1249.86	1191.27
F2000	0.82	0.83	949.00	1001.91	1123.32	1106.20	1030.61
F2400	0.99	1.00	805.78	883.14	930.38	923.17	858.22
F2800	1.15	1.16	670.58	760.79	763.90	698.31	697.00
F3200	1.32	1.33	555.50	640.52	591.57	582.21	566.87
F3600	1.48	1.50	462.51	527.03	478.98	469.83	469.58
F4000	1.64	1.66	388.68	427.08	413.82	400.49	391.62

**Table 5** Buckling load of the back-to-back compound channel sections (pinned ends)

Label	EC3	AISI	$P_{design}(kN)$		$P_{num}(kN)$		
	$\bar{\lambda}$	$\lambda_c$	EC3	AISI	S=50 mm	S=100 mm	S=200 mm
P400	0.33	0.33	1281.69	1274.83	1395.62	1392.28	1378.26
P600	0.49	0.50	1191.08	1203.77	1365.65	1369.56	1355.53
P800	0.66	0.67	1081.12	1110.88	1264.63	1278.78	1245.85
P1000	0.82	0.83	949.00	1001.91	1059.37	1043.88	1090.27
P1200	0.99	1.00	805.78	883.14	944.04	856.14	929.11
P1400	1.15	1.16	670.58	760.79	717.58	766.64	748.95
P1600	1.32	1.33	555.50	640.52	610.75	607.61	599.04
P1800	1.48	1.50	462.51	527.03	504.71	499.39	492.54
P2000	1.64	1.66	388.68	427.08	409.29	413.93	409.37

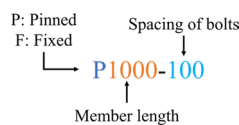


**Fig. 11** Labelling of the strut member (example of the 1000-mm long member with pinned ends and spacing of bolt equal to 100 mm)

## 5 Numerical Parametric Analysis

To investigate the behaviour of the back-to-back compound section, numerical parametric analysis was conducted on the full-scale cross-section described in Sect. 3, using the modelling approach validated in the previous section. The parametric analysis was aimed at investigating the buckling resistance of the back-to-back compound sections and evaluating the reliability of current codified design procedures.

The CFS strut members involved in the parametric analysis was summarised in Table 4 and 5 for fixed and pinned boundary conditions, respectively. For convenience, the rules shown in Fig. 11 was adopted to label each strut member included in the parametric analysis. The lengths of the strut members with fixed ends ranged from 800 to 4000 mm, which were twice the lengths of the pinned-end members.

Correspondingly the fixed-end members and the pinned-end members were associated with the same range of slenderness, which was between 0.33 and 1.64 in terms of the EC3 non-dimensional slenderness, or between 0.33 and 0.64 in terms of the AISI slenderness. Besides, as also shown in Table 4 and 5, for the fixed-end members, bolt spacings equal to 100, 200 and 400 mm were considered in this study, while for the pinned-end members, the adopted bolt spacings were 50, 100 and 200 mm. Notably, a sensitivity analysis on the size of mesh, similar to the one introduced in Sect. 4.2, was also conducted prior to the numerical parametric analysis. It was found that a mesh size of 4 mm was sufficient to achieve relatively accurate results and at the same time able to reduce the computational demand.

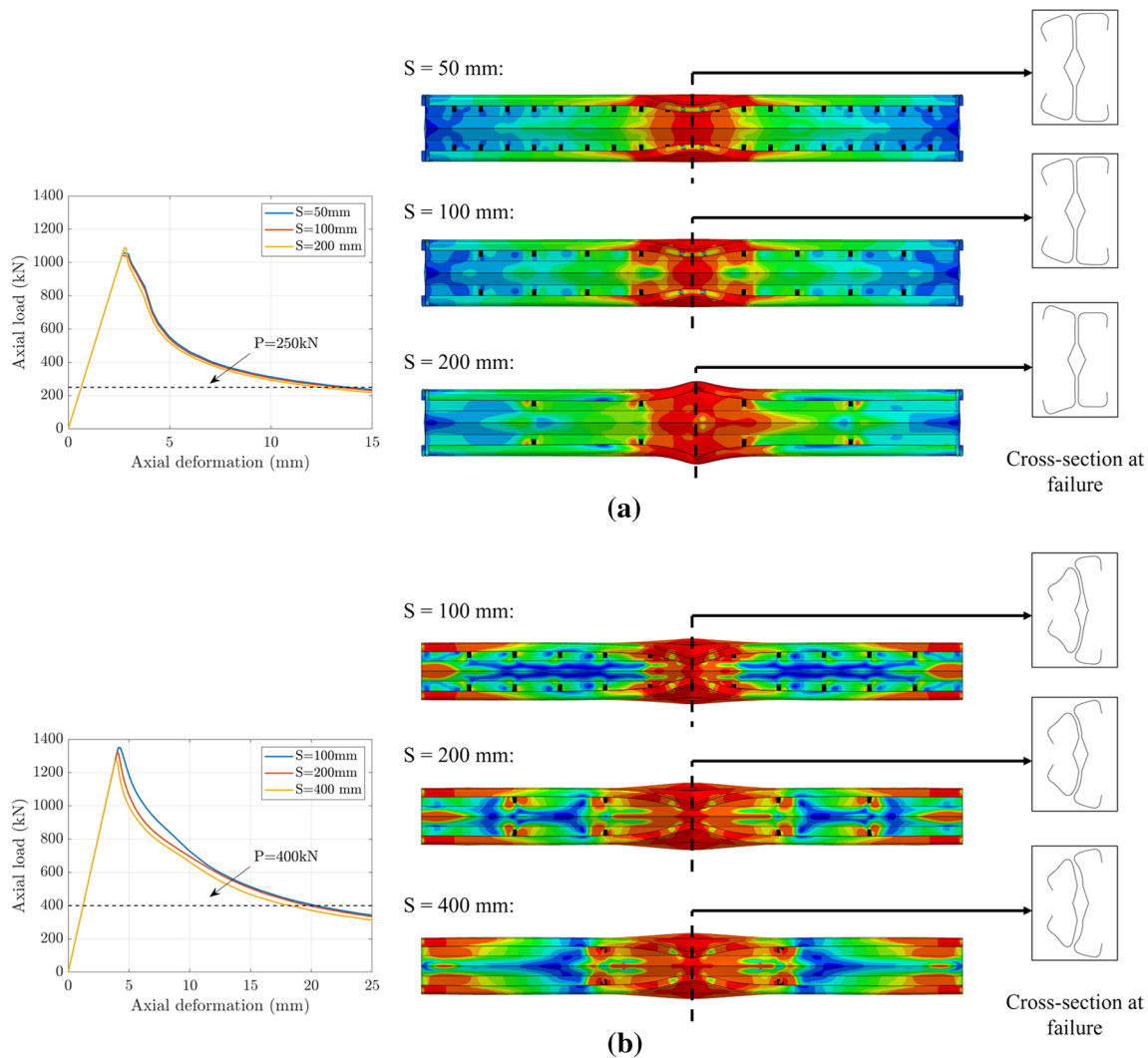
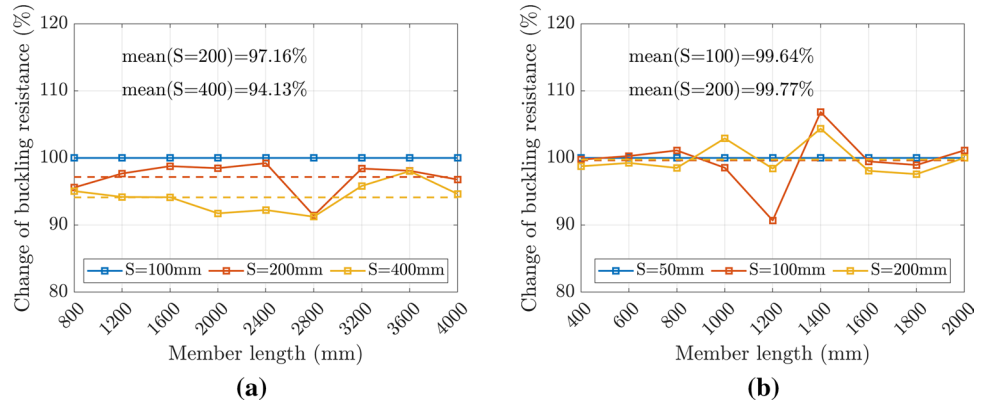


Fig. 12 Representative failure mechanisms of strut members: **a** the P1000 members; **b** the F1200 members

**Fig. 13** Comparisons of member buckling resistance with different bolt spacings: **a** fixed ends; **b** pinned ends



**5.1 Behaviour of the CFS Members**

The behaviour of the CFS members was presented and discussed in this section, with attention also paid to the effects of spacing of bolts. Figure 12 shows the representative failure mechanisms of the strut members analysed in this study, where the black dots in the members represent the locations of bolts. Figure 12a presents the shape of the P1000 members when the residual loads were equal to 250 kN, approximately 25% of the peak load. The predominant buckling modes of this group of members were flexural buckling about the weak axis with slight effects from distortional buckling. It can be seen that the increasing spacing of bolts

did affect the stress distribution in the web of the failure area, however, either the predominant buckling mode or the size of the failure area were in general not affected. Nevertheless, some high stress concentrations were observed around the bolts in the P1000-200 members, suggesting potential local damage around the bolts or failure of the bolts. Such stress concentrations were not found in the other two P1000 members. Figure 12b shows the failure modes of the F1200 members, whose behaviour was predominantly controlled by combined flexural and distortional buckling. It can be seen that despite all three F1200 members have similar shape at failure, the small bolt spacing seemed to have restrained the area of the member that underwent inelastic deformation. In

**Fig. 14** Comparisons of the numerical buckling resistance with the EC3 design buckling curve

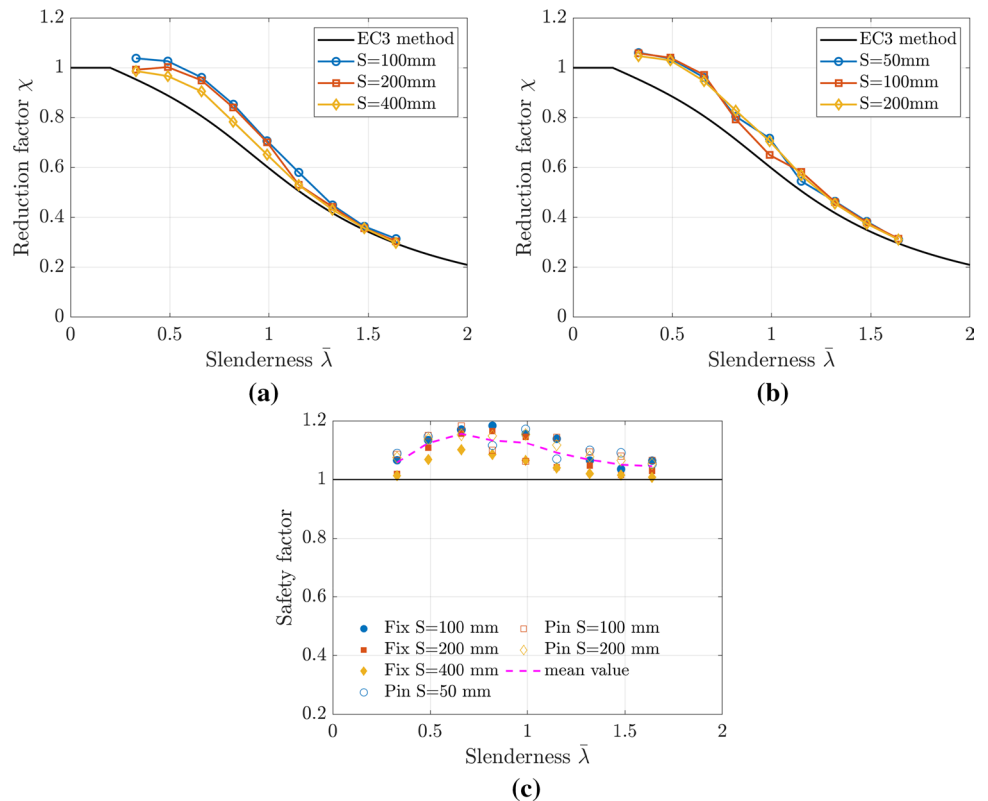
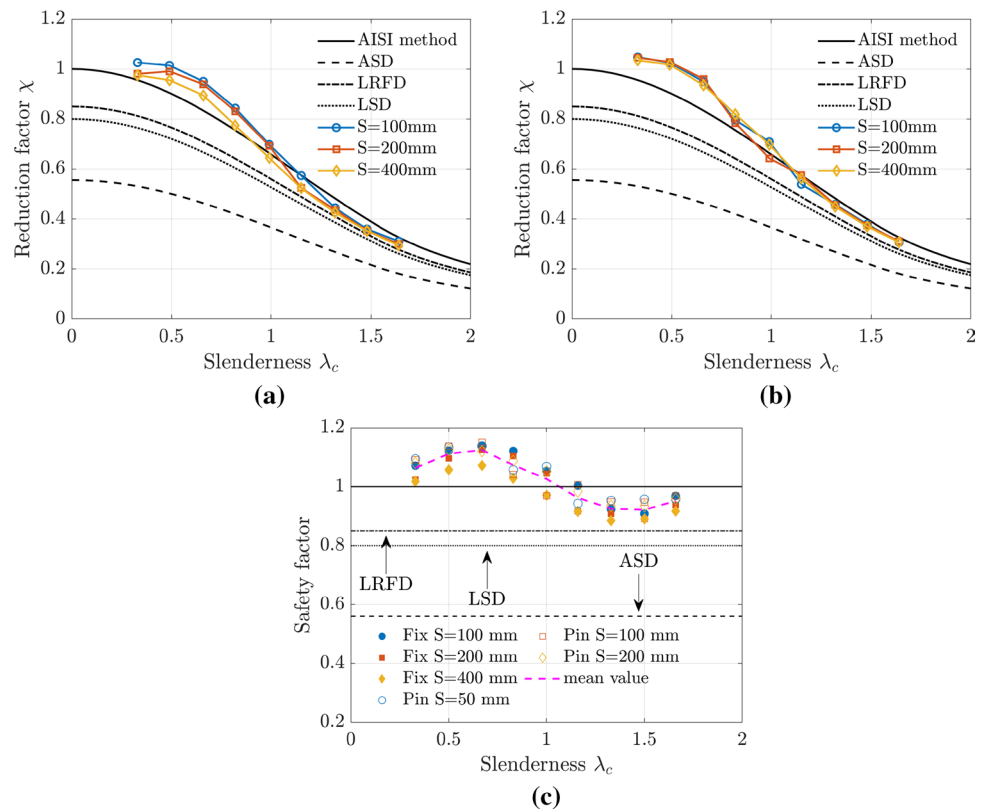


**Fig.15** Comparisons of the numerical buckling resistance with the AISI design buckling resistance



addition, high stress concentration was also noticed around the bolts in the F1200-200 and F1200-400 members, similar to the case of P1000-400 member shown in Fig. 12a.

Figure 13 shows the variation of member buckling load due to increased spacing of bolts. In general, it can be seen that the increase of bolt spacing did not significantly change the member buckling load, as the variations were all within 10% for both the fixed-end and pinned-end members. The limited variation could be explained by the different local buckling modes due to different spacings of bolts, which had some effects on the imperfection of the FE models in this study. However, as the change of bolt spacing did not alter the predominant buckling mode, the variation in buckling loads were not significant. As shown in Fig. 13a, for fixed-end members, increasing the spacing of bolt from 100 to 200 and 400 mm on average led to a 3 and 6% reduction in the buckling load, respectively. On the other hand, as indicated in Fig. 13b, the variation of buckling load of the pinned-end members were considered negligible, hence the use of more bolts was not necessarily beneficial to the member buckling resistance in this study.

## 5.2 Assessment of Standardised Design Procedure

A preliminary assessment of the EC3 and the AISI design procedures was carried out in this study by comparing the design buckling loads with the numerical results. The results

are presented in Figs. 14 and 15. The design buckling load was determined based on the methods introduced in Sect. 2. It should be mentioned during the assessment of the EC3 design method, as shown in Fig. 14, the design load was presented in terms of the reduction factor  $\chi$ , hence the numerical results were normalised by the compressive capacity of each member, as demonstrated by Eq. (8). In a similar manner, as illustrated in Fig. 15, the buckling resistance obtained by the AISI method could also be expressed as a design buckling curve based on Eq. (1) in Table 1, as it has been mentioned in Sect. 3 that the effects of local and distortional buckling can be ignored for the compound section investigated in the present study. Correspondingly, the numerical results were normalised according to Eq. (9) in this case. It is essential to mention that the yield stress adopted in the codified design (denoted as  $f_y$ ) was the characteristic value equal to 700 MPa, hence was different from the yield stress implemented in the FE models, which took the mean value based on previous experiments equal to 764 MPa, as mentioned in Sect. 4.2. Moreover, the implementation of the EC3 method utilised the buckling curve b (See in Fig. 1) to calculate the design buckling load, which was based on the general shape of the back-to-back compound channel section.

$$\chi = P_{num} / A_{eff} f_y \quad (8)$$

$$P_{num}/P_y = P_{num}/A_g f_y \quad (9)$$

The comparisons between the buckling loads obtained numerically and using EC3 method are presented in Fig. 14. As can be seen, the EC3 design approach provided safe design values for all the strut members involved in the numerical analysis. Figure 14c also shows the margin of safety through the use of safety factors, which were defined as the ratio between the numerical buckling load and the design buckling load. The mean value of safety factors shows that the EC3 method tended to yield more conservative design values for members with slenderness  $\bar{\lambda}$  in the range between 0.5 and 1.0, where the mean safety factor is around 1.13. For stocky members with slenderness  $\bar{\lambda}$  smaller than 0.5, the safety factor dropped towards 1.0 as the effects of buckling became limited. Additionally, for more slender members ( $\bar{\lambda} > 1.0$ ), the corresponding mean safety factor was gradually reduced to approximately 1.05. Considering that the partial factor  $\gamma_{M1}$  used in the EC3 method to reduce the design value for redundancy, as shown in Eq. (1), is equal to 1.0, the EC3 method can be unsafe for some of strut members in this study, especially those with fixed ends and 400-mm spacing of bolt.

The assessment of the AISI method is presented in Fig. 15. It was found that when considering the unfactored buckling loads, the buckling loads estimated by the AISI method were on average around 10% higher than the numerical results for the strut members with slenderness  $\lambda_c$  less than 1.0, with the highest safety factor found to be around 1.12 for the P800-100 member. However, for members with  $\lambda_c$  larger than 1.0, the AISI method overestimated the buckling loads by an average of around 5%, with the lowest one being around 0.88 for the F3200-400 member. Nevertheless, this does not mean that AISI method is not safe in this case. The AISI method also requires the use of factored resistance based on different requirements, as shown in Eq. (10) including the Allowable Strength Design (ASD), Load and Resistance Factor Design (LRFD) and Limit States Design (LSD) Requirements. It can be seen in Fig. 15 that the AISI method eventually led to safe buckling design for the strut members considered in this study.

$$P = P_n / \Omega_c = \phi_c P_n$$

$$\text{where } P_n = \min\{P_{ne}, P_{nl}, P_{nd}\}$$

$$\Omega_c = 1.80 \text{ for ASD}$$

$$\phi_c = 0.85 \text{ for LRFD}$$

$$\phi_c = 0.80 \text{ for LSD}$$

(10)

## 6 Conclusions

This paper presented a numerical parametric study on a back-to-back CFS compound channel section made of S700 steel, aiming at evaluating the reliability of codified design methods. FE models were established and validated against experimental test results, which were then adapted in the parametric analysis.

The following conclusions can be drawn based on the results of the numerical parametric analysis:

- The spacings of bolts was able to influence the high stress concentration in the failure area of the members
- The spacings of bolts exhibited limited impact on the buckling loads of the members in this study, mainly due to the change in initial imperfection
- The EC3 method provided safe design for all the members considered, and was more conservative for members with slenderness between 0.5 and 1.0
- The AISI method overestimated the buckling loads of the members with slenderness over 1.0 when no factors were used, however, it yielded safe design for all the members when factored buckling loads were considered.

Additional experimental and numerical simulations are, however, needed to enhance the reliability of current design practice and existing building codes for the efficient use of CFS channel sections for ordinary and temporary construction structural systems.

**Funding** The present research has been funded through a collaborative program between the Temporary Works forum (TWF) in the UK and the Civil Engineering and Industrial Design at University of Liverpool. The first two Authors would like to express their gratitude to TWF for their financial contribution.

## Declarations

**Conflict of interest** The authors have no competing interests to declare that are relevant to the content of this article.

**Open Access** This article is licensed under a Creative Commons Attribution 4.0 International License, which permits use, sharing, adaptation, distribution and reproduction in any medium or format, as long as you give appropriate credit to the original author(s) and the source, provide a link to the Creative Commons licence, and indicate if changes were made. The images or other third party material in this article are included in the article's Creative Commons licence, unless indicated otherwise in a credit line to the material. If material is not included in the article's Creative Commons licence and your intended use is not permitted by statutory regulation or exceeds the permitted use, you will need to obtain permission directly from the copyright holder. To view a copy of this licence, visit <http://creativecommons.org/licenses/by/4.0/>.



## References

- American Iron and Steel Institute (AISI). (2016). AISI S100–16 North American specification for the design of cold-formed steel structural members. AISI, Washington, DC, USA.
- ASTM International. (2019). ASTM E9 standard test methods of compression testing of metallic materials at room temperature. ASTM, West Conshohocken, Pennsylvania, USA.
- Becque, J., & Rasmussen, K. J. (2009). Experimental investigation of local-overall interaction buckling of stainless steel lipped channel columns. *Journal of Constructional Steel Research*, *65*(8–9), 1677–1684. <https://doi.org/10.1016/j.jcsr.2009.04.025>
- Chan, T. M., Zhao, X. L., & Young, B. (2015). Cross-section classification for cold-formed and built-up high strength carbon and stainless steel tubes under compression. *Journal of Constructional Steel Research*, *106*, 289–295. <https://doi.org/10.1016/j.jcsr.2014.12.019>
- Chen, B., Roy, K., Uzzaman, A., Raftery, G. M., Nash, D., Clifton, G. C., Pouladi, P., & Lim, J. B. (2019). Effects of edge-stiffened web openings on the behaviour of cold-formed steel channel sections under compression. *Thin-Walled Structures*, *144*, 106307. <https://doi.org/10.1016/j.tws.2019.106307>
- Craveiro, H. D., Rodrigues, J. P., & Laím, L. (2016). Buckling resistance of axially loaded cold-formed steel columns. *Thin-Walled Structures*, *106*, 358–375. <https://doi.org/10.1016/j.tws.2016.05.010>
- Dabaon, M., Ellobody, E., & Ramzy, K. (2015a). Experimental investigation of built-up cold-formed steel section battened columns. *Thin-Walled Structures*, *92*, 137–145. <https://doi.org/10.1016/j.tws.2015.03.001>
- Dabaon, M., Ellobody, E., & Ramzy, K. (2015b). Nonlinear behaviour of built-up cold-formed steel section battened columns. *Journal of Constructional Steel Research*, *110*, 16–28. <https://doi.org/10.1016/j.jcsr.2015.03.007>
- Ellobody, E., & Young, B. (2005). Behavior of cold-formed steel plain angle columns. *Journal of Structural Engineering*, *131*(3), 457–466. [https://doi.org/10.1061/\(ASCE\)0733-9445\(2005\)131:3\(457\)](https://doi.org/10.1061/(ASCE)0733-9445(2005)131:3(457))
- Ghannam, M. (2017). Axial load capacity of cold-formed steel built-up stub columns. *International Journal of Steel Structures*, *17*(4), 1273–1283. <https://doi.org/10.1007/s13296-017-1202-0>
- Haidarali, M. R., & Nethercot, D. A. (2012). Local and distortional buckling of cold-formed steel beams with both edge and intermediate stiffeners in their compression flanges. *Thin-Walled Structures*, *54*, 106–112. <https://doi.org/10.1016/j.tws.2012.02.013>
- Hancock, G. J., Murray, T., & Ellifrit, D. S. (2001). *Cold-formed steel structures to the AISI specification*. CRC Press.
- Kesti, J., & Davies, J. M. (1999). Local and distortional buckling of thin-walled short columns. *Thin-Walled Structures*, *34*(2), 115–134. [https://doi.org/10.1016/S0263-8231\(99\)00003-8](https://doi.org/10.1016/S0263-8231(99)00003-8)
- Kwon, Y. B., Kim, B. S., & Hancock, G. J. (2009). Compression tests of high strength cold-formed steel channels with buckling interaction. *Journal of Constructional Steel Research*, *65*(2), 278–289. <https://doi.org/10.1016/j.jcsr.2008.07.005>
- Lian, Y., Uzzaman, A., Lim, J. B., Abdelal, G., Nash, D., & Young, B. (2016a). Effect of web holes on web crippling strength of cold-formed steel channel sections under end-one-flange loading condition—Part I: Tests and finite element analysis. *Thin-Walled Structures*, *107*, 443–452. <https://doi.org/10.1016/j.tws.2016.06.025>
- Lian, Y., Uzzaman, A., Lim, J. B., Abdelal, G., Nash, D., & Young, B. (2016b). Effect of web holes on web crippling strength of cold-formed steel channel sections under end-one-flange loading condition—Part II: Parametric study and proposed design equations. *Thin-Walled Structures*, *107*, 489–501. <https://doi.org/10.1016/j.tws.2016.06.026>
- Rahnavard, R., Craveiro, H. D., Laím, L., Simões, R. A., & Napolitano, R. (2021). Numerical investigation on the composite action of cold-formed steel built-up battened columns. *Thin-Walled Structures*, *162*, 107553. <https://doi.org/10.1016/j.tws.2021.107553>
- Rasmussen, K. J., & Hancock, G. J. (1994). Design of thin-walled plain channel section columns against flexural buckling. *Thin-Walled Structures*, *20*(1–4), 219–240. [https://doi.org/10.1016/0263-8231\(94\)90067-1](https://doi.org/10.1016/0263-8231(94)90067-1)
- Roy, K., Mohammadjani, C., & Lim, J. B. (2019b). Experimental and numerical investigation into the behaviour of face-to-face built-up cold-formed steel channel sections under compression. *Thin-Walled Structures*, *134*, 291–309. <https://doi.org/10.1016/j.tws.2018.09.045>
- Roy, K., Ting, T. C. H., Lau, H. H., & Lim, J. B. (2018a). Nonlinear behaviour of back-to-back gapped built-up cold-formed steel channel sections under compression. *Journal of Constructional Steel Research*, *147*, 257–276. <https://doi.org/10.1016/j.jcsr.2018.04.007>
- Roy, K., Ting, T. C. H., Lau, H. H., & Lim, J. B. (2018b). Effect of thickness on the behaviour of axially loaded back-to-back cold-formed steel built-up channel sections: Experimental and numerical investigation. *Structures*, *16*, 327–346. <https://doi.org/10.1016/j.istruc.2018.09.009>
- Roy, K., Ting, T. C. H., Lau, H. H., & Lim, J. B. (2019a). Experimental and numerical investigations on the axial capacity of cold-formed steel built-up box sections. *Journal of Constructional Steel Research*, *160*, 411–427. <https://doi.org/10.1016/j.jcsr.2019.05.038>
- Standard Australia (SA). (2018). *AS/NZS 4600:2018 Cold-formed steel structures*. Standard Australia, Sydney, Australia.
- Schafer, B. W. (2020). CUFSM software Version 5.04, Department of Civil Engineering, Johns Hopkins University, USA.
- Schafer, B. W., & Peköz, T. (1998). Computational modeling of cold-formed steel: Characterizing geometric imperfections and residual stresses. *Journal of Constructional Steel Research*, *47*(3), 193–210. [https://doi.org/10.1016/S0143-974X\(98\)00007-8](https://doi.org/10.1016/S0143-974X(98)00007-8)
- Shakil, S., Lu, W., & Puttonen, J. (2020). Experimental studies on mechanical properties of S700 MC steel at elevated temperatures. *Fire Safety Journal*, *116*, 103157. <https://doi.org/10.1016/j.firesaf.2020.103157>
- Shu, G., Zheng, B., & Shen, X. (2013). Experimental and theoretical study on the behavior of cold-formed stainless steel stub columns. *International Journal of Steel Structures*, *13*(1), 141–153. <https://doi.org/10.1007/s13296-013-1013-x>
- Dassault Systemes. (2014). Abaqus 6.14 Documentation. Simulia Systems, Providence, RI, USA.
- The European Committee for Standardization (CEN). (2005). *Eurocode 3: design of steel structures - Part 1-1: General rules and rules for buildings*. BSI, London, UK.
- The European Committee for Standardization (CEN). (2006). *Eurocode 3: design of steel structures - Part 1-3: General rules - Supplementary rules for cold-formed members and sheeting*. BSI, London, UK.
- Ting, T. C. H., Roy, K., Lau, H. H., & Lim, J. B. (2018). Effect of screw spacing on behavior of axially loaded back-to-back cold-formed steel built-up channel sections. *Advances in Structural Engineering*, *21*(3), 474–487. <https://doi.org/10.1177/1369433217719986>
- Yan, J., & Young, B. (2002). Column tests of cold-formed steel channels with complex stiffeners. *Journal of Structural Engineering*, *128*(6), 737–745. [https://doi.org/10.1061/\(ASCE\)0733-9445\(2002\)128:6\(737\)](https://doi.org/10.1061/(ASCE)0733-9445(2002)128:6(737))

- Yang, D., & Hancock, G. J. (2004). Compression tests of high strength steel channel columns with interaction between local and distortional buckling. *Journal of Structural Engineering*, 130(12), 1954–1963. [https://doi.org/10.1061/\(ASCE\)0733-9445\(2004\)130:12\(1954\)](https://doi.org/10.1061/(ASCE)0733-9445(2004)130:12(1954))
- Ye, J., Hajirasouliha, I., & Becque, J. (2018). Experimental investigation of local-flexural interactive buckling of cold-formed steel channel columns. *Thin-Walled Structures*, 125, 245–258. <https://doi.org/10.1016/j.tws.2018.01.020>
- Young, B., & Rasmussen, K. J. (1998a). Tests of fixed-ended plain channel columns. *Journal of Structural Engineering*, 124(2), 131–139. [https://doi.org/10.1061/\(ASCE\)0733-9445\(1998\)124:2\(131\)](https://doi.org/10.1061/(ASCE)0733-9445(1998)124:2(131))
- Young, B., & Rasmussen, K. J. (1998b). Design of lipped channel columns. *Journal of Structural Engineering*, 124(2), 140–148. [https://doi.org/10.1061/\(ASCE\)0733-9445\(1998\)124:2\(140\)](https://doi.org/10.1061/(ASCE)0733-9445(1998)124:2(140))
- Zhang, J. H., & Young, B. (2012). Compression tests of cold-formed steel I-shaped open sections with edge and web stiffeners. *Thin-Walled Structures*, 52, 1–11. <https://doi.org/10.1016/j.tws.2011.11.006>

**Publisher's Note** Springer Nature remains neutral with regard to jurisdictional claims in published maps and institutional affiliations.